(Received 22 April 2026, Accepted 22 May 2026, Scheduled 28 May 2026)

Discrete Space Vector Modulation Model Predictive Flux Control with Reformulated Incremental Cost Function and Efficient Search Strategy for SPMSM

Yang Zhang*, Jiahao Zhang, Ping Yang, Wancheng Xie, and Ziyi Wushao

Hunan University of Technology, Zhuzhou 412007, China

ABSTRACT: Conventional model predictive flux control (C-MPFC) generates large steady-state ripples, and the system reference values are heavily dependent on the permanent magnet (PM) flux. This paper proposes a discrete space-vector modulation model predictive flux control with a reformulated incremental cost function and efficient search strategy (RDSVM-MPFC) for surface-mounted permanent magnet synchronous motors (SPMSMs). First, a unified cost function based on flux increments is reconstructed by redefining the d-axis reference flux. Second, the candidate set is expanded via discrete space vector modulation (DSVM) in the spatial flux increment plane to generate a set of virtual flux increment vectors (VFIVs), thereby significantly suppressing steady-state errors. Furthermore, to manage the heavy computation burden associated with the expanded VFIVs, a three-stage hierarchical optimization strategy is designed. This approach achieves rapid identification of the optimal control vector, which preserves the high steady-state precision while largely reducing the computational complexity of the system. Finally, experimental studies demonstrate that the proposed RDSVM-MPFC strategy eliminates sensitivity to PM flux variations and markedly suppresses steady-state pulsations.

1. INTRODUCTION

Permanent magnet synchronous motors (PMSMs) are widely used in various industrial sectors due to their high efficiency, excellent control performance, and high power density [1, 2]. To achieve high-performance regulation of PMSMs, modern control strategies are required to ensure fast dynamic responses and maintain steady-state precision under complex constraints across the entire speed range. Field-oriented control (FOC) and direct torque control (DTC) are two classical control strategies applied in industrial applications. FOC achieves the decoupled control of torque and flux through coordinate transformations, but its performance relies heavily on the careful tuning of proportional-integral (PI) controllers [3]. DTC directly controls the stator flux and electromagnetic torque without inner current loops. This provides a simplified architecture, excellent robustness, and fast dynamic responses [4]. However, traditional DTC suffers from large torque and flux ripples, which limit its application in high-precision scenarios. Recently, model predictive control (MPC) has emerged as a highly effective control strategy in motor drives. It features an intuitive concept, fast dynamic responses, and the easy handling of multivariable constraints [5, 6]. Model predictive current control (MPCC) and model predictive torque control (MPTC) are the two main categories of MPC [7, 8]. Compared to MPCC, MPTC preserves the excellent transient capability of DTC. However, the torque and stator flux variables in the MPTC cost function have different units and magnitudes. Consequently, MPTC performance depends heavily on the careful tuning of weighting factors [9]. This tuning process often relies on empirical trial-and-error procedures and lacks systematic theoretical guidance, which severely limit the control accuracy and robustness of MPTC under complex operating conditions [10]. To address this issue, ranking-based strategies [11] and fuzzy decision logic [12] have been introduced. However, these methods significantly increase the computational burden and implementation complexity. Additionally, offline-tuned fixed weighting factors struggle to maintain optimal performance across the entire operation range due to the strong coupling of motor states [13]. An online optimization scheme based on torque ripple minimization was proposed in [14], but its performance depends heavily on accurate motor parameters. To eliminate the tedious tuning of weighting factors entirely, model predictive flux control (MPFC) was introduced [15]. MPFC converts the reference torque and stator flux amplitude into an equivalent reference stator flux vector. Therefore, the constraints in the cost function have the same units and magnitudes. This strategy eliminates the weighting factors while inheriting the fast dynamic responses and low torque ripples of MPTC [16]. Although MPFC inherently eliminates weighting factors, its control performance relies heavily on the accuracy of the predictive model. In practical applications, factors such as temperature drift, magnetic saturation, and measurement errors inevitably cause parameter mismatches [17]. These parameter variations and unmodeled dynamics act as lumped disturbances. They cause prediction errors in the stator flux, which leads the system to selecting non-optimal voltage vectors during the sampling period. To address this, existing studies frequently utilize

* Corresponding author: Yang Zhang (459387623@qq.com).

parameter identification [18] or disturbance observers [19–21]. Despite these improvements, traditional MPFC still faces inherent limitations. The calculation of the equivalent stator flux reference depends heavily on the precise knowledge of the permanent magnet (PM) flux. Furthermore, parameter variations easily disturb the calculation of the reference load angle, which degrades the overall steady-state accuracy of the PMSM system. Moreover, the steady-state performance of conventional MPFC is limited because a standard two-level inverter only provides eight basic voltage vectors [22]. To overcome this limitation, virtual voltage vectors (VVVs) were introduced in [23]. The synthesis of virtual vectors expands the finite control set, providing more candidate vectors for cost function evaluation. Discrete space vector modulation (DSVM) is an effective synthesis strategy, but it introduces a massive computational burden due to candidate vector enumeration [24]. Researchers have explored various methods to balance computational overhead and control performance. For example, a deadbeat principle was used in [25] to estimate the reference vector and locally evaluate only three adjacent vectors in the space vector plane. In [26], auxiliary lines were introduced to streamline the optimization process. Although these methods reduce the number of iterations, they are heavily coupled with deadbeat algorithms. This coupling reduces the system's robustness against parameter disturbances and complicates the control logic. To alleviate the high computational complexity associated with the expanded virtual vector set in DSVM, various pre-selection and search-reduction strategies have been investigated in recent literature. For instance, a highly efficient voltage vector selection method was proposed in [27] for induction motor drives. By utilizing the boundary positions of the unconstrained optimal voltage vector, it mathematically reduces the candidate set from 38 to 15 vectors without sacrificing any suboptimality, while also optimizing the switching frequency. To address the aforementioned challenges, this paper proposes a discrete space vector modulation model predictive flux control with a reformulated incremental cost function and efficient search strategy (RLDSVM-MPFC) for SPMSM. By redefining the d-axis reference flux vector, the proposed method eliminates the dependence of conventional MPFC on PM flux parameters. On this basis, a new cost function of flux increments is reconstructed to reduce control complexity. A spatial flux vector plane is utilized to intuitively analyze the flux variations induced by different switching states. To mitigate the steady-state errors caused by a limited control set, virtual flux vectors are introduced to expand the candidate set. Concurrently, to alleviate the ensuing computational burden, a three-stage hierarchical optimization scheme is formulated. Rapid optimal vector selection is achieved by the real-time iteration of the cost function. The primary contributions of this research are summarized below:

1) In the proposed RDSVM-MPFC strategy, the d-axis reference flux is redefined. This makes the system reference values independent of the PM flux. Consequently, it effectively enhances system robustness against PM parameter variations. Furthermore, the traditional C-MPFC cost function includes multiple variables, such as stator flux, voltage, and current. To address this, a new cost function is reconstructed using only flux increments, which significantly reduces control complexity.

2) The control set in C-MPFC contains only 8 vectors. This limitation causes severe steady-state torque ripples, flux ripples, and current distortion. To mitigate these issues, the proposed RDSVM-MPFC employs DSVM technology to expand the VFIVs. The expanded set contains 38 candidate fluxes. By applying the virtual flux vector plane to the new cost function, the optimal flux incremental vector can be intuitively selected. This method effectively suppresses steady-state errors and current distortion.

3) To alleviate the computational burden and sluggish dynamic response caused by the massive virtual flux control set, a three-stage optimal selection strategy is proposed. Stage 1: Six typical VFIVs from six sectors are evaluated in the reconstructed cost function to determine the optimal sector. Stage 2: Two basic flux incremental vectors within this sector are evaluated to identify the optimal triangle. Stage 3: All vectors within the optimal triangle are evaluated sequentially to determine the global optimal flux incremental vector.

The rest of this paper is organized as follows. The mathematical representation of the SPMSM and the fundamentals of C-MPFC are established in Section 2. The theoretical framework and implementation specifics of the proposed RDSVM-MPFC strategy are detailed in Section 3. Experimental results validating the effectiveness of the proposed strategy are provided in Section 4. Finally, the conclusions are drawn in Section 5.

2. MATHEMATICAL MODEL OF SPMSM AND C-MPFC

Within the d-q axis reference frame, the stator voltage for an SPMSM can be formulated as follows:

$$\begin{aligned} u_d &= R_s i_d - \omega_e \psi_q + \frac{d\psi_d}{dt} \\ u_q &= R_s i_q + \omega_e \psi_d + \frac{d\psi_q}{dt} \end{aligned} \tag{1}$$

The stator flux expressions are given by:

$$\begin{aligned} \psi_d &= L_d i_d + \psi_f \\ \psi_q &= L_q i_q \end{aligned} \tag{2}$$

where u_d, u_q, i_d, i_q, ψ_d, and ψ_q denote the d-q axis components of the stator voltage, current, and flux linkage, respectively. ω_e is the electrical angular velocity of the rotor; R_s is the stator resistance; ψ_f is the PM flux; and L_d, L_q are the d-q axis stator inductances.

In SPMSMs, render the d-q axis inductances identical ($L_d = L_q = L_s$). Consequently, the electromagnetic torque equation is simplified to:

$$T_e = \frac{3}{2} p_n \psi_f i_q \tag{3}$$

where p_n is the number of pole pairs.

The stator flux at the $k+1$ instant is predicted by applying the first-order forward Euler approximation to (1). The following discrete-time state-space model is thus obtained:

$$\psi_{dq}(k+1) = \begin{bmatrix} \psi_d(k+1) \\ \psi_q(k+1) \end{bmatrix} = \begin{bmatrix} \psi_d(k) + T_s\omega_e\psi_q(k) - R_sT_si_d(k) + T_su_d(k) \\ \psi_q(k) - T_s\omega_e\psi_d(k) - R_sT_si_q(k) + T_su_q(k) \end{bmatrix} \quad (4)$$

where $\psi_d(k+1)$ and $\psi_q(k+1)$ are the d-q axis components of the stator flux at the $k+1$ instant, and T_s is the control period.

An alternative representation for the electromagnetic torque model of the SPMSM is formulated as:

$$T_e = \frac{2P_n}{3L_s}|\psi_f| \times |\psi_s| \sin_\delta \quad (5)$$

Adopting $i_d = 0$ control method, the stator flux ψ_s^{ref} is determined by:

$$|\psi_s^{ref}| = \sqrt{\psi_f^2 + (\frac{2T_e^{ref}L_q}{3n_p\psi_f})^2} \quad (6)$$

The reference load angle θ_s^{ref} can be expressed as:

$$\theta_s^{ref} = \arcsin\left(\frac{L_sT_e^{ref}}{1.5p_n\psi_f\psi_s^{ref}}\right) \quad (7)$$

The reference stator flux ψ_s^{ref} is decomposed into d-q axis components, denoted as ψ_d^{ref} and ψ_q^{ref}, which can be expressed as:

$$\psi_s^{ref} = \begin{bmatrix} \psi_d^{ref} \\ \psi_q^{ref} \end{bmatrix} = \begin{bmatrix} |\psi_s^{ref}| \cos\theta_s^{ref} \\ |\psi_s^{ref}| \sin\theta_s^{ref} \end{bmatrix} \quad (8)$$

Owing to the one-step delay inherent in digital control systems, delay compensation is applied to (4) as follows:

$$[\psi_s(k+2)] = \begin{bmatrix} \psi_d(k+2) \\ \psi_q(k+2) \end{bmatrix} = \begin{bmatrix} \psi_d(k+1) + T_s\omega_e\psi_q(k+1) - R_sT_si_d(k+1) + T_su_d(k+1) \\ \psi_q(k+1) - T_s\omega_e\psi_d(k+1) - R_sTi_q(k+1) + T_su_q(k+1) \end{bmatrix} \quad (9)$$

The cost function utilized in CMPFC is established as:

$$g = \left|\psi_{dq}^* - \psi_{dq}(k+2)\right|^2 \quad (10)$$

3. THE PROPOSED RDSVM-MPFC STRATEGY

3.1. Redefinition of Reference Flux and Reformulated Cost Function

The performance of C-MPFC is heavily reliant upon the precision of PM flux ψ_f estimation. In C-MPFC, the reference stator flux ψ_s^{ref} is constructed directly from ψ_f as the core benchmark. However, during real-world motor operation, ψ_f readily undergoes deviations due to temperature elevation and magnetic saturation, thereby influencing the precise synthesis of the reference flux. Such parameter mismatches inevitably introduce inaccuracies in reference load-angle computation, which in turn diminish both the steady-state accuracy and overall robustness. Moreover, the prediction model expressed in (4) incorporates coupled terms involving the stator flux, voltages, currents, and stator resistance. In response to these challenges, this paper reformulates the references stator flux to eliminate dependence on ψ_f and introduces a new cost function formulated exclusively in terms of flux increments, thereby strengthening robustness to ψ_f parameter variations while streamlining the entire control process.

Based on (4), the predictive expression can be reorganized as:

$$\psi_{dq}(k+1) = \begin{bmatrix} \psi_d(k+1) \\ \psi_q(k+1) \end{bmatrix} = \begin{bmatrix} \psi_d(k) + T_s\omega_e\psi_q(k) - R_sT_si_d(k) + T_su_d(k) \\ \psi_q(k) - T_s\omega_e\psi_d(k) - R_sT_si_q(k) + T_su_q(k) \end{bmatrix} \quad (11)$$

where $\psi_{dss} = \psi_d - \psi_f$, ψ_{dss} is the new d axis reference flux.

Given that the PM flux ψ_f remains invariant within a single control cycle, (11) can be reformulated as:

$$\psi_{dqs}(k+1) = \begin{bmatrix} \psi_{ds}(k+1) \\ \psi_{qs}(k+1) \end{bmatrix} = \begin{bmatrix} \psi_{dss}(k) + T_s\omega_e\psi_q(k) - R_sT_s\frac{\psi_{dss}(k)}{L_s} + T_su_d(k) \\ \psi_q(k) - T_s\omega_e(\psi_{dss}(k)+\psi_f) - \frac{R_s}{L_s}\psi_q(k)T_s + T_su_q(k) \end{bmatrix} \quad (12)$$

where $\psi_{dqs}(k+1)$ is the new predicted stator flux at the $k+1$ instant.

The initial state of the stator flux at the k instant, denoted as $\psi_{dq0}(k)$, is formulated as:

$$\psi_{dq0}(k) = \begin{bmatrix} \psi_{d0}(k) \\ \psi_{qo}(k) \end{bmatrix} = \begin{bmatrix} \psi_{dss}(k) + T_s\omega_e\psi_q(k) - R_sT_s\frac{\psi_{dss}}{L_s}(k) \\ \psi_q(k) - T_s\omega_e(\psi_{dss}(k)+\psi_f) - \frac{R_s}{L_s}\psi_q(k)T_s \end{bmatrix} \quad (13)$$

Throughout the duration of the sampling period T_s, d-q axis flux increment $\Delta\psi_{dq}(k)$ is generated by the application of the stator voltage vector u_s at the kth instant. This increment is expressed as:

$$\Delta\psi_{dq}(k) = T_s\begin{bmatrix} u_d(k) \\ u_q(k) \end{bmatrix} \quad (14)$$

Consequently, (12) can be rewritten as:

$$\psi_{dqs}(k+1) = \psi_{dq0}(k) + \Delta\psi_{dq}(k) \quad (15)$$

Introducing a one-step computational delay, the prediction for the stator flux at the $k+2$ instant is projected as:

$$\psi_{dqs}(k+2) = \psi_{dq0}(k) + \Delta\psi_{dq}(k+1) \tag{16}$$

Thus, cost function (10) is replaced with the newly constructed flux variables as follows:

$$g = \left|\psi_{dqs}^{ref} - \psi_{dqs}(k+2)\right|^2 \tag{17}$$

By inserting (16) into (17), obtain the following expression:

$$g = \left|\psi_{dqs}^{ref} - \psi_{dq0}(k) - \Delta\psi_{dq}(k+1)\right|^2 \tag{18}$$

The flux increment $\Delta\psi_{dqs}^{ref}$ demanded by the initial flux $\psi_{dq0}(k)$ to follow the reference stator flux ψ_{dqs}^{ref} can be expressed as

$$\Delta\psi_{dqs}^{ref} = \psi_{dq}^{ref} - \psi_{dq0}(k) \tag{19}$$

Substituting (19) into (18), the incremental flux cost function based on the reselected control variables can be obtained as:

$$C = \left|\Delta\psi_{dqs}^{ref} - \Delta\psi_{dq}(k+1)\right|^2 \tag{20}$$

By reformulating the reference flux ψ_{dss}^{ref} control variables, indirect control of the d-axis flux is achieved. This circumvents the incorporation of the ψ_f into the reference calculation, thereby eliminating the inherent dependence of the C-MPFC on ψ_f and the associated calculation errors of the reference load angle. It fundamentally resolves the PM flux parameter mismatch and the resultant lack of robustness found in traditional methods. Notably, the core of the proposed reformulation strategy lies in eliminating the sensitivity to real-time fluctuations of the PM flux linkage ψ_f during motor operation. The value of ψ_f is obtained from the real-time flux estimation of the motor model. It does not depend on the initial value of ψ_f. Moreover, the newly formulated cost function substitutes the tracking of absolute flux errors with the tracking of flux increments. This strategy reduces control complexity and accelerates system response, while concurrently providing a direction for the subsequent selection of flux vectors.

3.2. Construction of Spatial Flux Increment Plane

To perform flux vector selection intuitively and efficiently, this paper introduces the spatial flux increment plane. The 8 switching states of the inverter S_n (000, 100, 110, 010, 011, 001, 101, and 111) correspond to eight basic flux increments in the spatial plane. The flux increments $\Delta\psi_n$ under each state can be calculated as follows:

$$\Delta\psi_n = \begin{bmatrix} \Delta\psi_d \\ \Delta\psi_q \end{bmatrix} = \begin{bmatrix} u_d \\ u_q \end{bmatrix} \cdot T_s = \frac{2}{3} V_{dc} T_s \cdot \begin{bmatrix} \cos\theta_r & \cos\left(\theta_r - \frac{2\pi}{3}\right) & \cos\left(\theta_r + \frac{2\pi}{3}\right) \\ -\sin\theta_r & -\sin\left(\theta_r - \frac{2\pi}{3}\right) & -\sin\left(\theta_r + \frac{2\pi}{3}\right) \end{bmatrix} \cdot \begin{bmatrix} S_a \\ S_b \\ S_c \end{bmatrix} \tag{21}$$

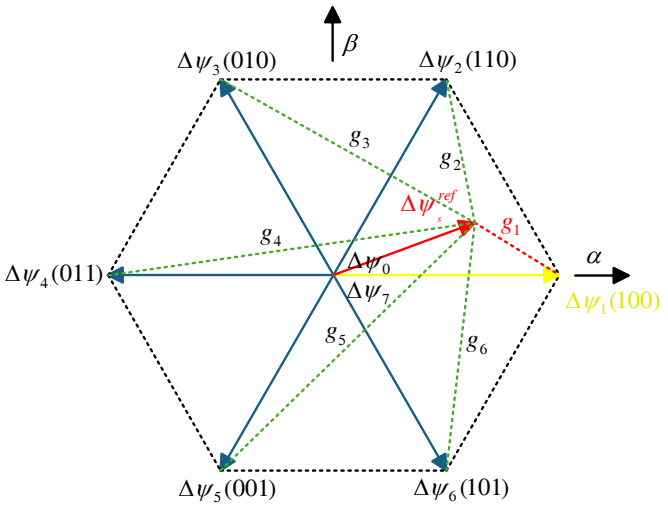

FIGURE 1. Spatial flux increment plane.

In the stationary coordinate system, the spatial flux increment plane is illustrated in Fig. 1.

Given the reference flux increment $\Delta\psi_s^{ref}$, the evaluation process of the cost function is simplified to compute the geometric distance between the reference flux increment and the candidate basic flux increments. As shown in the figure, the geometric distance between $\Delta\psi_s^{ref}$ and $\Delta\psi_n$ represents the cost function value g_n ($n = 0, 1 \ldots 7$). For instance, $\Delta\psi_1$ is the basic flux increment with the minimum distance error to the given reference flux increment $\Delta\psi_s^{ref}$. Therefore, g_1 serves as the optimal output solution of the cost function, and $\Delta\psi_1$ is selected as the optimal switching state applied at the $k+1$ instant. The introduction of the spatial plane makes the screening logic of voltage vectors intuitive, reducing the computational complexity of the system.

3.3. DSVM Virtual Flux Increment

Although the plane search in the flux increment plane is efficient, since the control set of basic flux increments contains only 8 finite vectors, the limited control set inevitably introduces non-negligible selection errors during the optimal solution screening process. This error maps into the time domain as pronounced torque ripples and increased current harmonics distortion. To address this, this paper proposes the concept of Discrete Space Vector Modulation Virtual Flux Increment vectors (VFIVs). By synthesizing new increment directions within the spatial plane, the original control set of 8 basic flux increments is expanded to 38. The VFIVs can reduce the total harmonic distortion (THD). The distribution of the VFIVs is illustrated in Fig. 2.

The unified expression for the VFIVs set can be expressed as:

$$\Delta\psi_{vir} = \sum_{i=1}^{3} x_i \Delta\psi_n \tag{22}$$

where $n = 0, 1, \ldots 7$, $x_i \in \{0, \frac{1}{3}, \frac{2}{3}\}$, $\sum x_i = 1$.

The synthesis mechanisms for virtual flux increment are categorized as follows:

TABLE 1. Virtual flux increments vectors synthesized by real flux increment vectors.

VFIV	Synthesis of actual flux increment vectors	VFIV	Synthesis of actual flux increment vectors
$\Delta\psi_8$	$(\Delta\psi_1+2\Delta\psi_0)/3$	$\Delta\psi_9$	$(\Delta\psi_2+2\Delta\psi_0)/3$
$\Delta\psi_{10}$	$(\Delta\psi_3+2\Delta\psi_0)/3$	$\Delta\psi_{11}$	$(\Delta\psi_4+2\Delta\psi_0)/3$
$\Delta\psi_{12}$	$(\Delta\psi_5+2\Delta\psi_0)/3$	$\Delta\psi_{13}$	$(\Delta\psi_6+2\Delta\psi_0)/3$
$\Delta\psi_{14}$	$(2\Delta\psi_1+\Delta\psi_0)/3$	$\Delta\psi_{16}$	$(2\Delta\psi_2+\Delta\psi_0)/3$
$\Delta\psi_{18}$	$(2\Delta\psi_3+\Delta\psi_0)/3$	$\Delta\psi_{20}$	$(2\Delta\psi_4+\Delta\psi_0)/3$
$\Delta\psi_{22}$	$(2\Delta\psi_5+\Delta\psi_0)/3$	$\Delta\psi_{24}$	$(2\Delta\psi_6+\Delta\psi_0)/3$
$\Delta\psi_{15}$	$(\Delta\psi_1+\Delta\psi_2+\Delta\psi_0)/3$	$\Delta\psi_{17}$	$(\Delta\psi_2+\Delta\psi_3+\Delta\psi_0)/3$
$\Delta\psi_{19}$	$(\Delta\psi_3+\Delta\psi_4+\Delta\psi_0)/3$	$\Delta\psi_{21}$	$(\Delta\psi_4+\Delta\psi_5+\Delta\psi_0)/3$
$\Delta\psi_{23}$	$(\Delta\psi_5+\Delta\psi_6+\Delta\psi_0)/3$	$\Delta\psi_{25}$	$(\Delta\psi_6+\Delta\psi_1+\Delta\psi_0)/3$
$\Delta\psi_{26}$	$(2\Delta\psi_1+\Delta\psi_2)/3$	$\Delta\psi_{27}$	$(\Delta\psi_1+2\Delta\psi_2)/3$
$\Delta\psi_{28}$	$(2\Delta\psi_2+\Delta\psi_3)/3$	$\Delta\psi_{29}$	$(\Delta\psi_2+2\Delta\psi_3)/3$
$\Delta\psi_{30}$	$(2\Delta\psi_3+\Delta\psi_4)/3$	$\Delta\psi_{31}$	$(\Delta\psi_3+2\Delta\psi_4)/3$
$\Delta\psi_{32}$	$(2\Delta\psi_4+\Delta\psi_5)/3$	$\Delta\psi_{33}$	$(\Delta\psi_4+2\Delta\psi_5)/3$
$\Delta\psi_{34}$	$(2\Delta\psi_5+\Delta\psi_6)/3$	$\Delta\psi_{35}$	$(\Delta\psi_5+2\Delta\psi_6)/3$
$\Delta\psi_{36}$	$(2\Delta\psi_6+\Delta\psi_1)/3$	$\Delta\psi_{37}$	$(\Delta\psi_6+2\Delta\psi_1)/3$

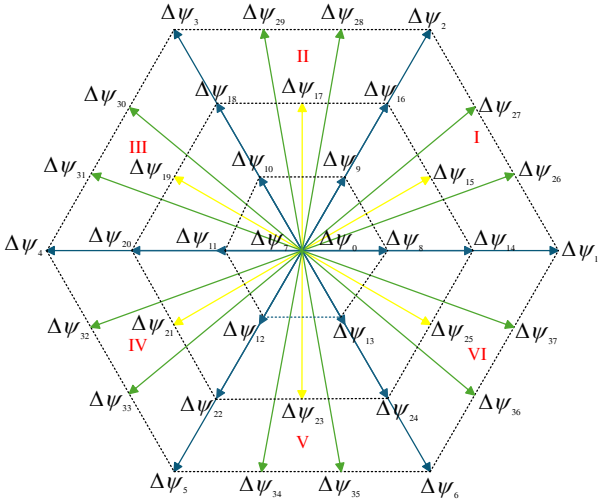

FIGURE 2. Spatial distribution of flux increment.

1) The first category of virtual flux increment vectors is a linear combination of a basic flux increment vector and a flux increment vector generated by zero voltage, such as $\Delta\psi_8$ and $\Delta\psi_9$.

2) The second category of virtual flux increment vectors is synthesized by the linear combination of two adjacent basic flux increment vectors. For example, $\Delta\psi_{26}$ and $\Delta\psi_{27}$ are linearly combined from $\Delta\psi_1$ and $\Delta\psi_2$, and so forth.

3) The third category of virtual flux increment vectors is a linear combination of two adjacent virtual flux increment vectors and a flux increment vector generated by zero voltage, like $\Delta\psi_{15}$ or $\Delta\psi_{17}$.

Based on the synthesis rules introduced above, the remaining VFIVs can also be synthesized. Table 1 details the synthesis specifics for all VFIVs.

3.4. Proposed Three-Stage Hierarchical Optimization Strategy

To balance the contradiction between the improved control precision brought by virtual flux increment expansion and aggravated computational burden, this paper proposes a selection strategy based on three-stage hierarchical optimization.

Stage I, 6 typical virtual flux increment vectors $\Delta\psi_n$ (n = 15, 17, 19, 21, 23, 25) are selected as the initial control set. By applying the cost function minimization criterion, the sector (I-VI) where the optimal vector resides is rapidly identified, thereby roughly demarcating the interval range of the optimal solution.

Stage II, taking the optimal vector determined in Stage I as a benchmark, if the optimal vector from Stage I is $\Delta\psi_{15}$, two adjacent basic flux increment vectors, $\Delta\psi_1$ and $\Delta\psi_2$, in the corresponding Sector I are selected for cost function evaluation. Based on the evaluation results, the search range is further narrowed down, retaining only the 6 candidate vectors within the targeted triangular region.

Stage III, following the selection strategies of Stage I and Stage II, the globally optimal flux increment vector is confined to a single right-angled triangle. For example, if the local optimal vector from Stage II is $\Delta\psi_2$, the candidate vectors $\Delta\psi$, $\Delta\psi_2$, $\Delta\psi_7\Delta\psi_9$, $\Delta\psi_{15}$, $\Delta\psi_{16}$, and $\Delta\psi_{27}$ within that right-angled triangle are sequentially substituted into the cost function to determine the globally optimal flux increment vector that minimizes the cost.

Through the proposed efficient selection process of flux increment vectors, only 13 candidate flux vector increments need to be evaluated in a single control period. Compared to eval-

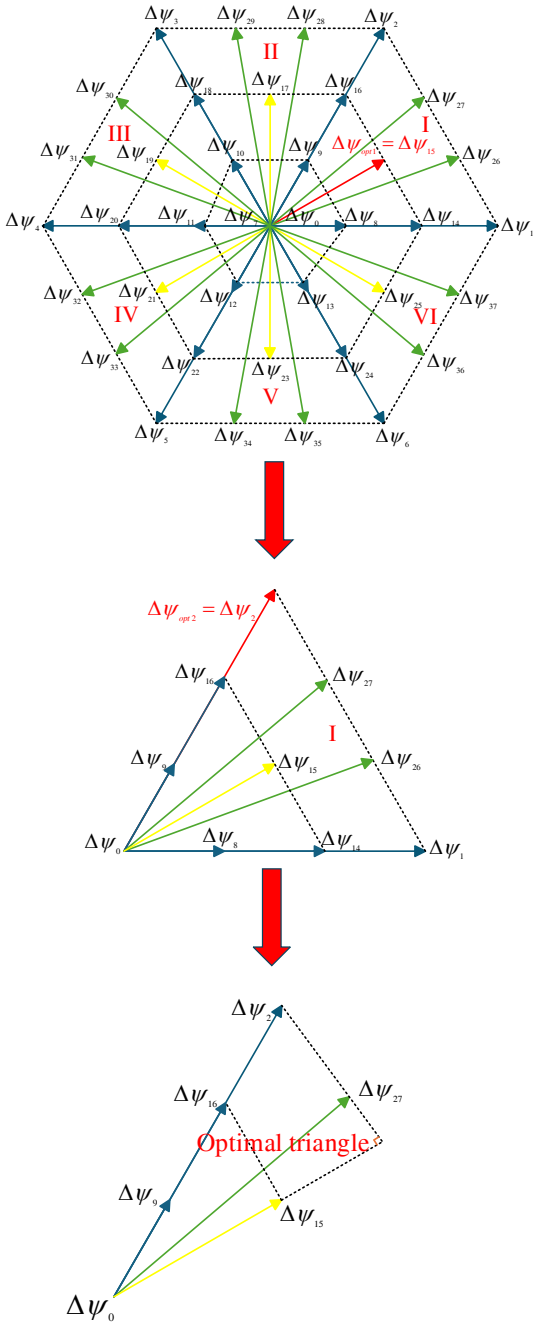

FIGURE 3. The optimization process of flux increment.

uating all 38 candidate voltage vectors, this strategy significantly alleviates the computational burden on the system and improves system response speed, and the diagram of the optimization process is shown in Fig. 3. Finally, the control block diagram of the proposed RDSVM-MPFC is illustrated in Fig. 4.

4. EXPERIMENTAL RESULTS AND CONCLUSION

To evaluate the practical performance of the proposed control strategy, a hardware-in-the-loop testbench based on RT-LAB was established, as depicted in Fig. 5. A TMS320F2812 digital signal processor (DSP) serves as the controller for this test system, while the SPMSM, inverter, and associated parameters are emulated by the RT-LAB simulator. The nominal parameters of

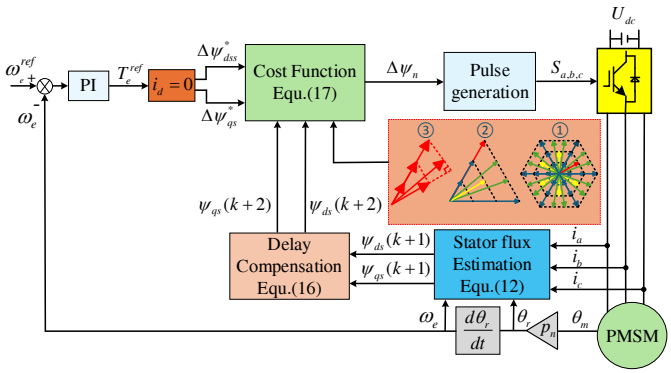

FIGURE 4. Block diagram of RDSVM-MPFC control system.

TABLE 2. Parameters of SPMSM.

Parameters	Values	Unit
Stator resistance (R_s)	0.15	Ω
Stator inductance (L_s)	1.625	(H)
Moment of inertia (J)	4.78e-3	(kg · m^2)
Rated torque (T_N)	15	(N · m)
PM flux (W_b)	0.1	(Wb)
DC bus voltage (U_{dc})	300	(V)
Pole pairs (P_n)	4	

the motor are detailed in Table 2. In this experiment, the sampling and control period T_s is set to 100 µs, which corresponds to a sampling frequency of 10 kHz.

In the experiments, the proposed Discrete Space Vector Modulation Model Predictive Flux Control (RDSVM-MPFC) and Reformulated Cost Function Model Predictive Flux Control (R-MPFC) are strictly compared with the conventional Model Predictive Flux Control (C-MPFC) in [16]. All comparisons are performed under identical parameters.

4.1. Steady-State Experimental Analysis

The waveforms acquired from the execution of the C-MPFC, R-MPFC, and the proposed RDSVM-MPFC algorithms are displayed in Fig. 6. In the steady-state experiments of Section 4.1, these analyses were conducted under the operating conditions of a target speed of 1000 r/min and a load torque of 10 N · m. Within each subplot, the waveforms corresponding to rotor speed, stator flux magnitude, electromagnetic torque, and phase-A current are arranged sequentially from top to bottom.

Based on the observations from Fig. 6, under steady-state operation, the proposed RDSVM-MPFC achieves a 62.5% reduction in torque ripple and a 66% reduction in flux ripple relative to the C-MPFC. This performance enhancement stems primarily from the extended virtual flux-increment vectors (VFIFs) together with the efficient search strategy proposed in this paper, both of which markedly strengthen the overall steady-state performance. In addition, the R-MPFC achieves steady-state performance identical to that of the C-MPFC. This confirms that the reselection of reference flux variables exerts no influence on control performance.

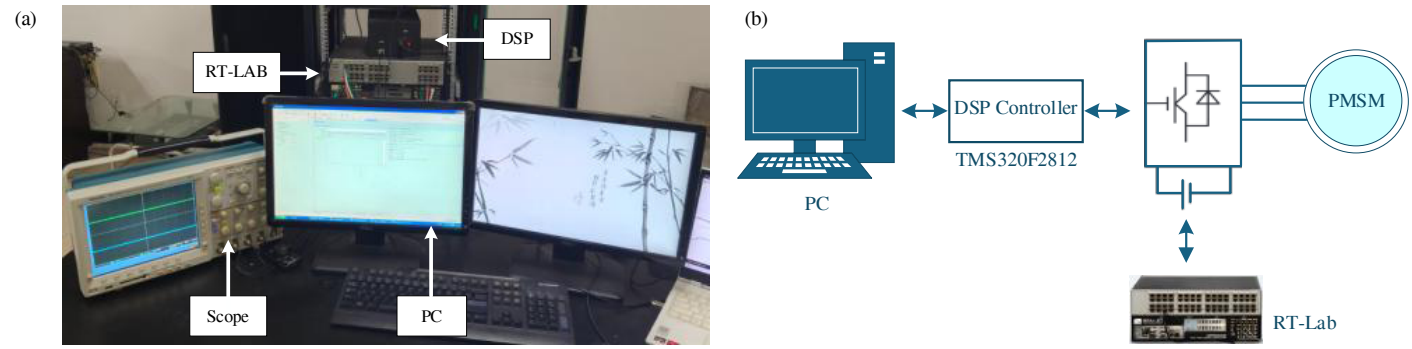

FIGURE 5. RT-LAB experiment platform. (a) Hardware t layout. (b) RT-LAB hardware-in-the-loop architecture.

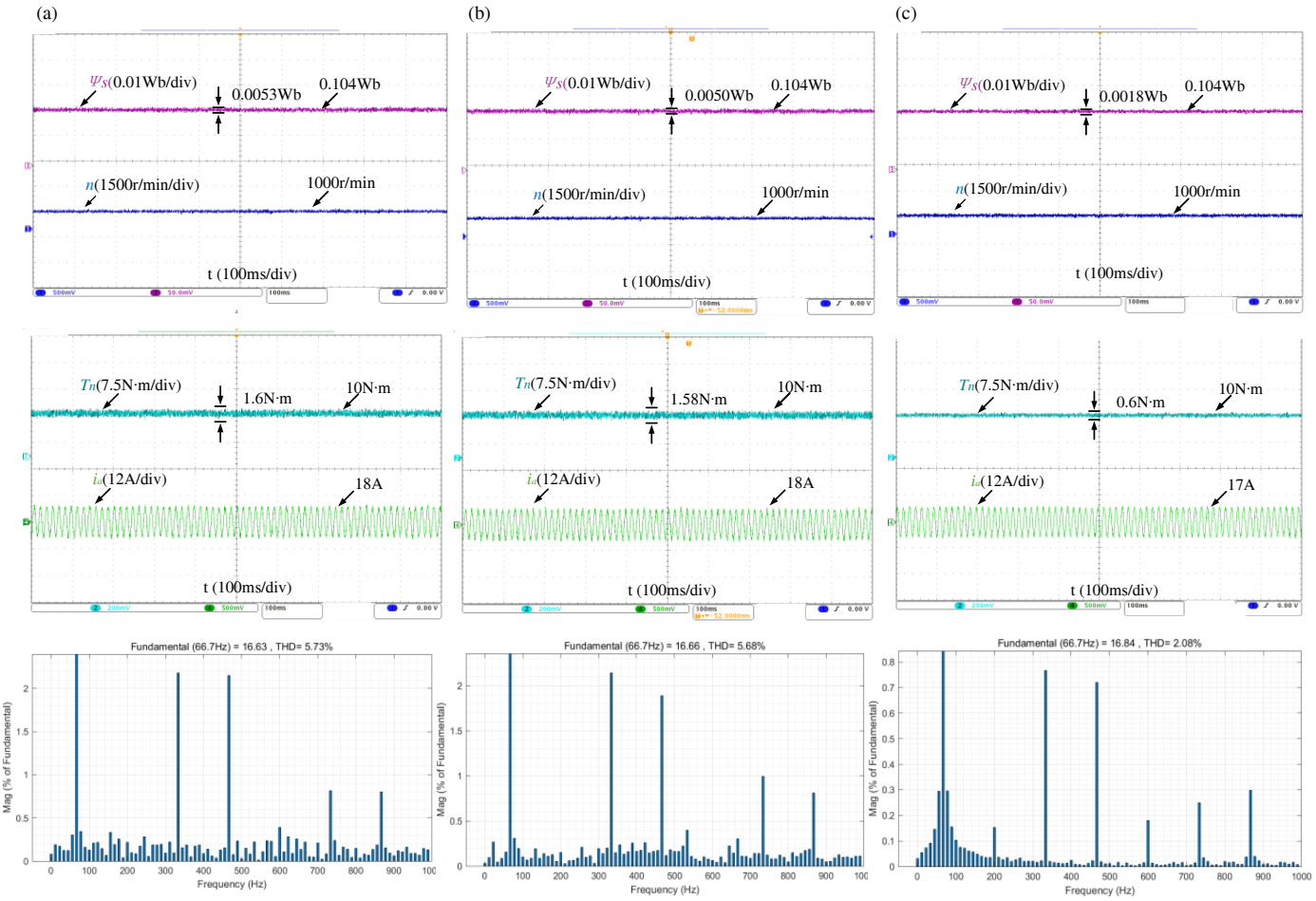

FIGURE 6. Steady-state experimental waveforms. (a) C-MPFC. (b) R-MPFC. (c) RDSVM-MPFC.

4.2. PM Flux Step Experimental Analysis

Figure 7 illustrates the sensitivity tests of the three strategies to variations in the PM flux ψ_f. In the first group of experiments, based on a nominal value of 0.1 Wb, ψ_f increases by 15% at 0.2 s and decreases by 15% at 0.7 s. Additionally, in the second group of experiments, based on a nominal value of 0.1 Wb, ψ_f increases by 30% at 0.2 s and decreases by 30% at 0.7 s. As shown in Fig. 7(a), the average d-axis current deviates, and the phase-A current magnitude changes in C-MPFC when ψ_f varies. This indicates that C-MPFC performance is highly dependent on permanent magnet parameters. Conversely, for the R-MPFC strategy in Fig. 7(b), phase-A and d-axis currents remain constant during ψ_f fluctuations. Since the reconstructed flux reference in R-MPFC is independent of ψ_f, the phase-A current, d-axis current, and torque are nearly unaffected, achieving offset-free tracking. Furthermore, in Fig. 7(c), the proposed RDSVM-MPFC strategy inherits the robustness of R-MPFC against ψ_f variations. It significantly reduces d-axis current ripple and only requires smaller three-phase currents to reach rated torque and rated speed.

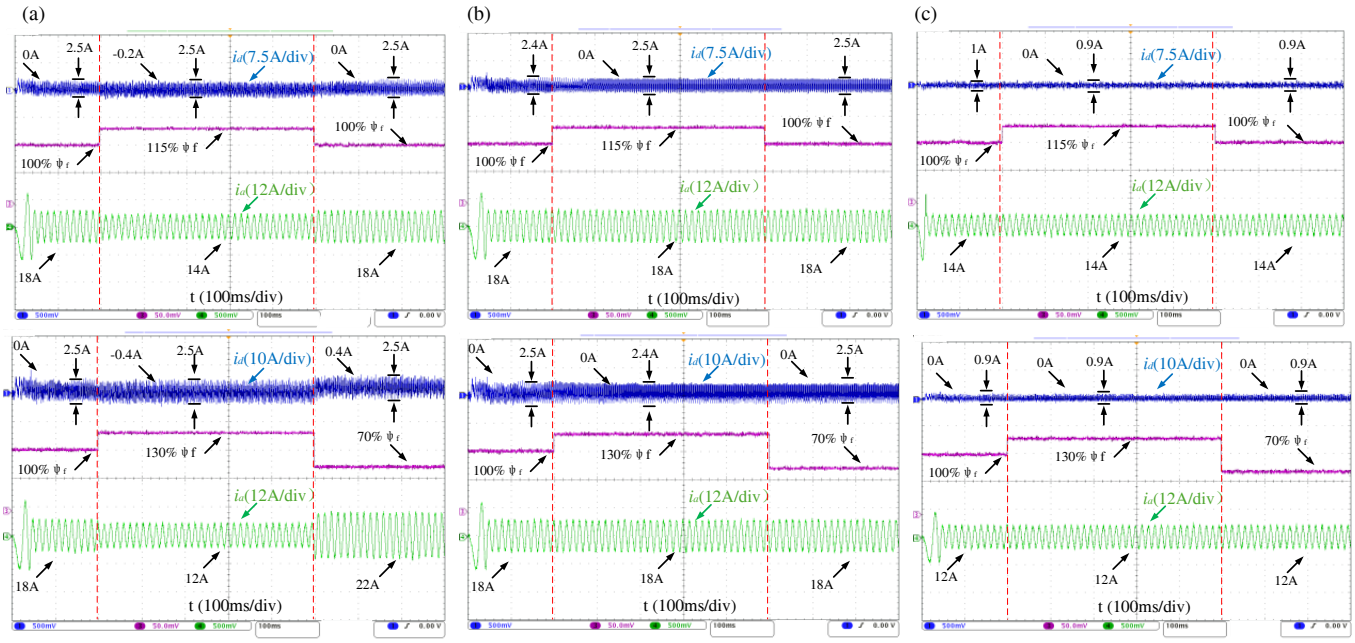

FIGURE 7. Experimental waveforms under PM flux step variations (a) C-MPFC. (b) R-MPFC. (c) RDSVM-MPFC.

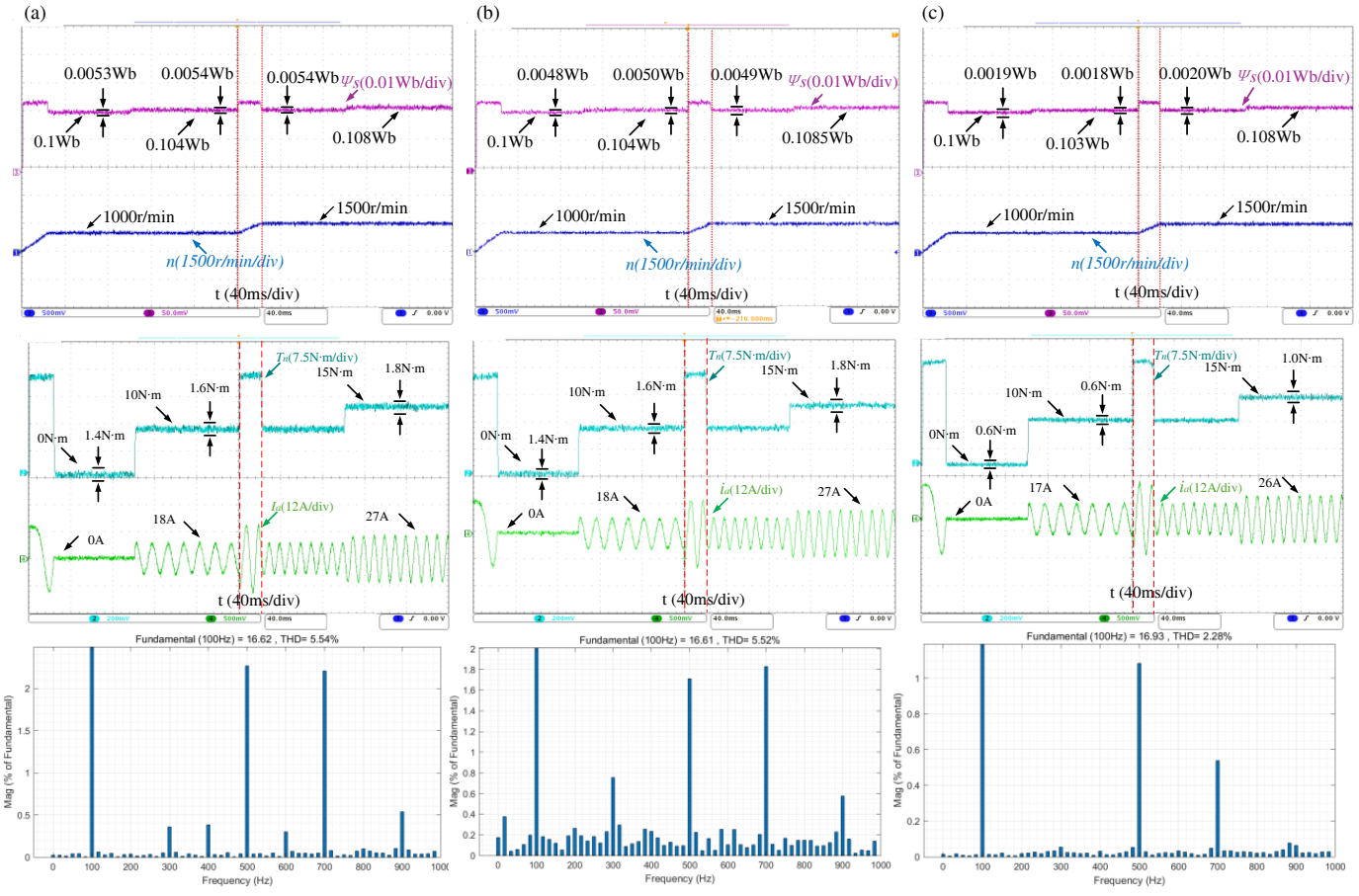

FIGURE 8. Dynamic experimental waveforms. (a) C-MPFC. (b) R-MPFC. (c) RDSVM-MPFC.

TABLE 3. Comparison of stator flux ripple, torque ripple, and THD.

Conditions	Methods	Flux ripple (Wb)	Torque ripple (N · m)	THD (%)
$n = 1000$ r/min $T_n = 10$ N · m	C-MPFC	0.0053 Wb	1.6 N · m	5.73%
	R-MPFC	0.0050 Wb	1.58 N · m	5.68%
	RDSVM-MPFC	0.0018 Wb	0.6 N · m	2.08%

4.3. Dynamic Experiment Analysis

As shown in Fig. 8, the dynamic test conditions is a no-load startup. The system reaches a rated speed of 1000 r/min and a rated torque of 10 N · m at 0.1 s. At 0.2 s, the speed accelerates to 1500 r/min. Finally, the load increases to 15 N · m at 0.3 s. The speed response performance is similar across all three control methods. The speed and torque dynamic responses of C-MPFC and R-MPFC are nearly identical. This demonstrates that redefining the reference flux does not degrade dynamic predictive performance. In contrast, the proposed RDSVM-MPFC produces a more stable phase-A current waveform with lower distortion and lower THD.

Experimental results indicate that R-MPFC eliminates parameter mismatches caused by ψ_f variations without degrading predictive performance. As indicated in Table 3, the proposed RDSVM-MPFC inherits this robustness while further reducing d-axis current ripple, torque ripple, stator flux ripple, and THD. Table 4 presents a computational complexity comparison among different methods. The benchmarks include the C-MPFC strategy with virtual space modulation without the selection algorithm and the PTC-DSVM strategy from [26]. As indicated in Table 4, the execution time of the proposed RDSVM-MPFC strategy is reduced by **45.26%** compared to the C-MPFC strategy without selection processing. Meanwhile, its execution time is comparable to that of the PTC-DSVM method in the literature. This validates the effectiveness of the three-stage selection strategy and further reduces system computational complexity.

TABLE 4. Computational complexity comparison and execution time.

Methods	Execution	Time reduction
C-MPFC	8483 µs	/
PTC-DSVM	4425 µs	47.8%
RDSVM-MPFC	46.43 µs	45.26%

5. CONCLUSION

To address the permanent magnet (PM) flux parameter sensitivity and high steady-state ripples in conventional model predictive flux control (C-MPFC), this paper proposes a discrete space vector modulation model predictive flux control with a reformulated incremental cost function and an efficient search strategy for SPMSM (RDSVM-MPFC). Based on the research and experimental results, the primary conclusions are as follows:

1) In the proposed RDSVM-MPFC strategy, the d-axis reference flux is redefined. The cost function is reformulated using flux increments, ensuring that the reference values are independent of the PM flux. This effectively enhances system robustness against parameter variations and reduces control complexity. Compared to C-MPFC, the d-axis current ripple is reduced by 60%.

2) To resolve the large torque and flux ripples in C-MPFC, the proposed RDSVM-MPFC utilizes discrete space vector modulation to expand the set of Virtual Flux Incremental Vectors (VFIVs). Steady-state experimental results show that this strategy significantly suppresses flux and torque pulsations while reducing total harmonic distortion (THD). Compared with C-MPFC, the torque ripple is reduced by 62.5%, flux ripple reduced by 66%, and THD reduced by 63.7%.

3) To mitigate the computational burden and potential dynamic delays caused by the large VFIVs, a three-stage optimal selection strategy is proposed. This method reduces the number of required VFIV evaluations by 34%. Experimental results verify that the proposed method maintains the same dynamic response speed and similar execution time to C-MPFC, proving the effectiveness of the theory.

ACKNOWLEDGEMENT

This work was supported by the Scientific Research Fund of Hunan Provincial Education Department under Grant Number 24A0395.

REFERENCES

[1] Luo, Y. and C. Liu, "Elimination of harmonic currents using a reference voltage vector based-model predictive control for a six-phase PMSM motor," *IEEE Transactions on Power Electronics*, Vol. 34, No. 7, 6960–6972, Jul. 2019.

[2] Ramesh, P. and N. C. Lenin, "High power density electrical machines for electric vehicles — Comprehensive review based on material technology," *IEEE Transactions on Magnetics*, Vol. 55, No. 11, 1–21, Nov. 2019.

[3] Navardi, M. J., J. Milimonfared, and H. A. Talebi, "Torque and flux ripples minimization of permanent magnet synchronous motor by a predictive-based hybrid direct torque control," *IEEE Journal of Emerging and Selected Topics in Power Electronics*, Vol. 6, No. 4, 1662–1670, Dec. 2018.

[4] Zhong, L., M. F. Rahman, W. Y. Hu, and K. W. Lim, "Analysis of direct torque control in permanent magnet synchronous motor drives," *IEEE Transactions on Power Electronics*, Vol. 12, No. 3, 528–536, May 1997.

[5] Alfaro, C., R. Guzman, L. G. d. Vicuña, J. Miret, and M. Castilla, "Dual-loop continuous control set model-predictive control for a three-phase unity power factor rectifier," *IEEE Transactions on Power Electronics*, Vol. 37, No. 2, 1447–1460, Feb. 2022.

[6] Preindl, M., "Robust control invariant sets and Lyapunov-based MPC for IPM synchronous motor drives," *IEEE Transactions on Industrial Electronics*, Vol. 63, No. 6, 3925–3933, Jun. 2016.

[7] Yuan, X., S. Zhang, C. Zhang, A. Galassini, G. Buticchi, and M. Degano, "Improved model predictive current control for SPMSM drives using current update mechanism," *IEEE Transactions on Industrial Electronics*, Vol. 68, No. 3, 1938–1948, Mar. 2021.

[8] Zhou, Z., C. Xia, Y. Yan, Z. Wang, and T. Shi, "Torque ripple minimization of predictive torque control for PMSM with extended control set," *IEEE Transactions on Industrial Electronics*, Vol. 64, No. 9, 6930–6939, Sep. 2017.

[9] Davari, S. A., D. A. Khaburi, and R. Kennel, "An improved FCS–MPC algorithm for an induction motor with an imposed optimized weighting factor," *IEEE Transactions on Power Electronics*, Vol. 27, No. 3, 1540–1551, Mar. 2012.

[10] Zhang, Y. and H. Yang, "Model predictive torque control of induction motor drives with optimal duty cycle control," *IEEE Transactions on Power Electronics*, Vol. 29, No. 12, 6593–6603, Dec. 2014.

[11] Rojas, C. A., J. Rodriguez, F. Villarroel, J. R. Espinoza, C. A. Silva, and M. Trincado, "Predictive torque and flux control without weighting factors," *IEEE Transactions on Industrial Electronics*, Vol. 60, No. 2, 681–690, Feb. 2013.

[12] Villarroel, F., J. R. Espinoza, C. A. Rojas, J. Rodriguez, M. Rivera, and D. Sbarbaro, "Multiobjective switching state selector for finite-states model predictive control based on fuzzy decision making in a matrix converter," *IEEE Transactions on Industrial Electronics*, Vol. 60, No. 2, 589–599, Feb. 2013.

[13] Davari, S. A., D. A. Khaburi, and R. Kennel, "Using a weighting factor table for FCS-MPC of induction motors with extended prediction horizon," in *IECON 2012 — 38th Annual Conference on IEEE Industrial Electronics Society*, 2086–2091, Montreal, QC, Canada, Oct. 2012.

[14] Cortes, P., S. Kouro, B. L. Rocca, R. Vargas, J. Rodriguez, J. I. Leon, S. Vazquez, and L. G. Franquelo, "Guidelines for weighting factors design in model predictive control of power converters and drives," in *2009 IEEE International Conference on Industrial Technology*, 1–7, Churchill, VIC, Australia, 2009.

[15] Zheng, Z. and D. Sun, "Model predictive flux control with cost function-based field weakening strategy for permanent magnet synchronous motor," *IEEE Transactions on Power Electronics*, Vol. 35, No. 2, 2151–2159, Feb. 2020.

[16] Zhang, Y., H. Yang, and B. Xia, "Model-predictive control of induction motor drives: Torque control versus flux control," *IEEE Transactions on Industry Applications*, Vol. 52, No. 5, 4050–4060, Sep.-Oct. 2016.

[17] Yan, L., M. Dou, and Z. Hua, "Disturbance compensation-based model predictive flux control of SPMSM with optimal duty cycle," *IEEE Journal of Emerging and Selected Topics in Power Electronics*, Vol. 7, No. 3, 1872–1882, Sep. 2019.

[18] Wang, Q., G. Wang, N. Zhao, G. Zhang, Q. Cui, and D. Xu, "An impedance model-based multiparameter identification method of PMSM for both offline and online conditions," *IEEE Transactions on Power Electronics*, Vol. 36, No. 1, 727–738, Jan. 2021.

[19] Mousavi, M. S., S. A. Davari, V. Nekoukar, C. Garcia, and J. Rodriguez, "A robust torque and flux prediction model by a modified disturbance rejection method for finite-set model-predictive control of induction motor," *IEEE Transactions on Power Electronics*, Vol. 36, No. 8, 9322–9333, Aug. 2021.

[20] Huang, S., G. Wu, F. Rong, C. Zhang, S. Huang, and Q. Wu, "Novel predictive stator flux control techniques for PMSM drives," *IEEE Transactions on Power Electronics*, Vol. 34, No. 9, 8916–8929, Sep. 2019.

[21] Hou, Q., S. Ding, and X. Yu, "Composite super-twisting sliding mode control design for PMSM speed regulation problem based on a novel disturbance observer," *IEEE Transactions on Energy Conversion*, Vol. 36, No. 4, 2591–2599, Dec. 2021.

[22] Chen, L., H. Xu, X. Sun, and Y. Cai, "Three-vector-based model predictive torque control for a permanent magnet synchronous motor of EVs," *IEEE Transactions on Transportation Electrification*, Vol. 7, No. 3, 1454–1465, Sep. 2021.

[23] Gao, L., J. E. Fletcher, and L. Zheng, "Low-speed control improvements for a two-level five-phase inverter-fed induction machine using classic direct torque control," *IEEE Transactions on Industrial Electronics*, Vol. 58, No. 7, 2744–2754, Jul. 2011.

[24] Gu, M., Y. Yang, M. Fan, Y. Xiao, P. Liu, X. Zhang, H. Yang, and J. Rodriguez, "Finite control set model predictive torque control with reduced computation burden for PMSM based on discrete space vector modulation," *IEEE Transactions on Energy Conversion*, Vol. 38, No. 1, 703–712, Mar. 2023.

[25] Wang, W., C. Liu, S. Liu, and H. Zhao, "Model predictive torque control for dual three-phase PMSMs with simplified deadbeat solution and discrete space-vector modulation," *IEEE Transactions on Energy Conversion*, Vol. 36, No. 2, 1491–1499, Jun. 2021.

[26] Wang, Y., X. Wang, W. Xie, F. Wang, M. Dou, R. M. Kennel, R. D. Lorenz, and D. Gerling, "Deadbeat model-predictive torque control with discrete space-vector modulation for PMSM drives," *IEEE Transactions on Industrial Electronics*, Vol. 64, No. 5, 3537–3547, May 2017.

[27] Osman, I., D. Xiao, M. F. Rahman, M. Norambuena, and J. Rodriguez, "Discrete space vector modulation based model predictive flux control with reduced switching frequency for IM drive," *IEEE Transactions on Energy Conversion*, Vol. 36, No. 2, 1357–1367, Jun. 2021.